RSC Advances

REVIEW

View Article Online
View Journal | View Issue

Cite this: *RSC Adv.*, 2026, **16**, 15814

Biochar beads as emerging adsorbents for water purification: mechanisms, performance, and applications

Himanshi Soni,[ab] Monika Bhattu,[b] Mikhael Bechelany [c] and Jagpreet Singh *[b]

The continuously growing interest in sustainable and innovative materials has driven the production of biochar-based bead adsorbents as recoverable and structurally stable alternatives to powdered biochar. Owing to their tunable physicochemical properties, enhanced mechanical stability, and cost-effectiveness, these materials have emerged as promising material for wastewater treatment applications. This review systematically evaluates recent advancements in the synthesis approaches, surface functionalization, and applications of biochar-based beads in wastewater treatment. The primary focus of the present work is to elucidate the adsorption mechanisms, including electrostatic interactions, surface complexation, π–π electron overlap, hydrogen bonding, ligand exchange, and redox processes that govern the adsorbent performance, with a focus on the oxygen-containing functional groups, polymer-derived functional groups, and aromatic domains in bead matrices that influence these mechanisms. The effects of key experimental parameters such as pH, adsorbent dosage, temperature, contact time, and initial pollutant concentration on adsorption efficiency are critically analyzed. In contrast to other review articles that broadly focus on biochar and its applications in wastewater treatment, the present review specifically focuses on biochar-based bead adsorbents, offering in-depth insights into their synthesis–structure–property relationships, adsorption behaviour, and regeneration potential. Furthermore, the review highlights current limitations and outlines future research directions aimed at enhancing selectivity, stability, scalability, and environmental sustainability.

Received 28th January 2026
Accepted 10th March 2026

DOI: 10.1039/d6ra00740f

rsc.li/rsc-advances

1. Introduction

Water pollution has emerged as a significant global health threat driven by industrialization and urbanization.[1–4] Industries often discharge large amounts of pollutants (dyes, heavy metals, pesticides, pharmaceuticals, and surfactants) directly into rivers, contaminating the water sources.[5–10] In addition to industrial waste, human activities such as agricultural practices, mining, and urban development also degrade water quality.[11–14] Synthetic dyes from textiles, paper, and printing industries are released in heavy amounts.[15] As stated by WHO, millions of people are suffering from health diseases due to lack of access to clean drinking water.[16] At present, nearly 2 billion people live in different regions experiencing water stress, while around 700 million people have no access to safe and clean drinking water.[17–20] Water is essential to human life, as it plays a crucial role in maintaining health and well-being.[21,22] However, limited access to pure and clean drinking water leads to significant health issues as the contaminated water carries several toxins that enter the human body.[23] Long-term exposure to such toxins has been associated with serious health issues, including cardiovascular disease and certain forms of cancer.[24,25] Researchers should focus on low-cost and sustainable technologies to mitigate the environmental and health risks attributed to these contaminants. To address water contaminants, several conventional processes have been introduced, such as ion exchange, coagulation, zeolite ion-exchanger resin, distillation, electrochemical methods, filtration, osmosis, and adsorption processes, which are some known processes utilized during wastewater treatment.[26–29] While these methods are effective to some extent, they often require high energy input and the use of toxic chemicals, reducing their overall sustainability and environmental compatibility. Among these, adsorption has gained considerable attention as it is one of the most effective and efficient methods that adsorb up to 99% the pollutants from wastewater with high efficiency.[30–32] Various adsorbents, such as activated carbon, metal oxides, polymeric composites, clay materials, and biochar have been extensively investigated for the removal of contaminants.[33–38] Among all these adsorbents, biochar is one of the well-known adsorbent identified for its high adsorption efficacy, attributed to its

[a]*Centre of Research Impact and Outcome, Chitkara University, Rajpura-140417, Punjab, India*

[b]*Bahra Research Innovation & Knowledge Cluster, Rayat Bahra University, Greater Mohali-140103, Punjab, India. E-mail: jagpreetnano@gmail.com*

[c]*Institut Européen des Membranes, IEM, UMR-5635, University of Montpellier, ENSCM, CNRS, Place Eugène Bataillon, CEDEX 5, 34095 Montpellier, France*

highly porous structure and high density of functional groups on its surface.[39–42] The ion exchange, surface precipitation, complexation, and electrostatic attraction are a few mechanisms that occur during the adsorption of pollutants on the surface of biochar.[43–45] Recent studies investigated the engineered materials for the development of biochar, such as magnetic biochar, biochar composites, and polymer-modified biochar composites, to improve the adsorption performance. For instance, Abdalla *et al.*, prepared biochar using pumpkin seeds for the efficient removal of organic pollutants. The study found that the removal rate reached 81.4% for RhB in 60 minutes.[46] Also, Kareem *et al.*, prepared biochar using apricot kernel cake as a natural precursor for the removal of Pb(II) and Cd(II) ions. The study states that chitosan-modified biochar achieved maximum adsorption capacity of 150.9 mg g^{-1} for Pb^{2+} ions and 149.3 mg g^{-1} for Cd^{2+} ions.[47] In another study, Kareem *et al.*, in 2025 developed magnetic biochar composites for the removal of Hg^{2+} and Cu^{2+} ions. The study found the maximum adsorption capacity of 141.89 mg g^{-1} for Hg^{2+} and 124.78 mg g^{-1} for Cu^{2+} ions.[48] Despite its effectiveness, biochar as an efficient adsorbent lacks large-scale applications due to its low regeneration ability.[15] To overcome this limitation, magnetic materials are introduced to increase the efficiency of biochar, as pristine biochar may not be suitable for regeneration processes.[49] The studies illustrate that incorporation of magnetic materials into biochar offers a promising approach for improving its separation efficacy.[50] Owing to their magnetic properties, magnetic biochar facilitates real-time applications, allowing the adsorbent to be easily recovered and reused. In addition to magnetization, modification of biochar using chemical and physical techniques are frequently utilized to further enhance the performance of biochar.[51,52] However, powdered form of biochar poses limited adsorption capacity and is somewhat complex to recover the powdered form of biochar.[53] Therefore, to address this issue, biochar-based beads have been prepared, offering high surface area and facilitating easy recovery from aqueous solution, making it a promising approach for the removal of contaminants.[54] In the preparation of such beads, natural polymers like sodium alginate, chitosan, and other natural-based polymers are utilized for the preparation of beads. Among these, sodium alginate binds are well known for their easy binding ability with other molecules present on the surface of biochar, enhancing the cross-linking reaction and strengthening the structure. Biochar beads formed through sodium alginate or chitosan which enhance the structural integrity and easy recovery. Although, synthesis of biochar beads reduces the surface area compared to the powdered form of biochar. Biochar beads offers accessibility towards functional groups, high mechanical stability, and porosity. Additionally, the inclusion of sodium alginate increases the size of biochar-based adsorbents, thus facilitating their separation from solution.[54] In this context, this review paper explores recent advancements in the use of biochar beads as adsorbents for water purification. Specifically, it explores the effect of different experimental conditions on the adsorption performance of biochar beads. Moreover, the review evaluates the effectiveness of biochar beads in adsorbing various pollutants and discusses their environmental impact. Although several review articles have discussed the synthesis methods, modification, and applications of biochar in wastewater treatment including adsorption mechanisms and surface engineering strategies. To the best of our knowledge, limited literature was found specifically on biochar-based bead adsorbents for water remediation. For instance, Olugbenga *et al.*, investigated the production methods of biochar and their applications in wastewater treatment.[55] Similarly, Aziz *et al.*, investigated various sources for the preparation of biochar, their modification techniques, and possible mechanisms for heavy metal removal.[10] In another instance, Díaz *et al.*, illustrated the synthesis techniques, properties, and modifications of biochar-based materials, focusing on their applications in wastewater treatment.[56] However, these studies primarily focus on the conventional powdered form of biochar instead of systematically analyzing bead-based adsorbents. The existing literature is still limited specifically to biochar-based bead adsorbents. The systematic understanding between beads composition, adsorption mechanisms, structural properties, and regeneration behavior have not been fully elaborated in existing literature. Biochar beads provide various positive attributes such as improved mechanical stability, easier separation from aqueous media, and better suitability for real water treatment systems. As a consequence, a thorough understanding of these materials is critical for improving their environmental applications. To bridge this gap, the current paper aims to highlight the recent developments in the preparation of biochar beads, with a particular focus on their role in enhancing adsorption capacity for wastewater treatment. By exploring this key aspect, the study evaluates the potential of biochar-based beads in environmental remediation and investigates how experimental parameters affect their adsorption performance, ultimately contributing to more sustainable water purification methods.

2. Synthesis techniques

With the continuously increasing interest in biochar bead-based adsorbents, various synthesis techniques have been developed to enhance the physicochemical properties and adsorption performance. This section includes the selection of raw materials with a focus on post-treatment and processing approaches.

2.1 Preparation of magnetic biochar beads

2.1.1 Raw materials. The primary source required during the preparation of biochar is biomass, which is derived from different organic sources.[57] The most common types of biomass utilized for the preparation of biochar include agricultural waste, forestry waste, and other solid wastes.[58,59] The selection of a particular biomass depends on the desired properties of the beads for wastewater treatment. On the other side, the synthesis of magnetic biochar beads includes magnetic materials such as iron oxide and iron salts, which are mixed with biomass during the pyrolysis process.[60,61] Additionally, natural and synthetic

binders are also added, which give a spherical shape to the beads. Iron-based materials are commonly used in the preparation of magnetic adsorbents due to their magnetic properties, which enable efficient separation and recovery of the beads from aqueous systems.[62] To enhance the interaction between biochar and magnetic particles, chemical precursors such as acids, alkalis, or metal salts are often introduced.[63] These precursors are utilized to improve the binding properties of magnetic particles. The preparation of a powdered form of biochar does not involve any gelation–calcination process. In contrast, the preparation of biochar-based beads includes a gelation–calcination process or cross-linking techniques to form stable, spherical beads.[64] Once the appropriate precursors are selected, further treatment is essential to ensure performance and reusability.

2.1.2 Post-treatment for magnetic biochar beads. Post-treatment is a critical step in ensuring the stability, reusability, and performance of magnetic biochar beads.[65] Several studies, therefore, have highlighted the effectiveness of various post-treatment processes in enhancing their adsorptive capabilities. For instance, Li *et al.*, investigated the preparation of MBC beads designed for the removal of humic acid. In this study, pretreatment of beads with peroxymonosulfate (PMS) has been done to improve the removal rate. The study observed that without adding PMS, humic acid led to significant fouling of the UF membrane, resulting in a final transmembrane pressure.[66] In contrast, when the pretreatment process was carried out, the removal rate increased with contact time. Moreover, the study illustrates the effect of the pretreatment process on the pH of the solution. Specifically, at high pH values, humic acid and polysaccharide organic pollutants are not dissolved in water. This is because the pretreatment affects the solubility by stabilizing the pollutants in a high pH values, owing to iron ion hydrolysis and weak acid generation.[66]

2.1.3 Gelation–calcination process for the preparation of beads. In the preparation of biochar-based beads, the gelation–calcination process is utilized, and the liquid mixture converts into a gel-like substance due to the presence of cross-linking agents.[67] Typically, biochar-based beads involve combining biochar with alginate (gel-forming substance) or other biopolymers and some add magnesium or iron ions.[68,69] In this process, the gel-like structure forms when the polymer chain cross-links, resulting in a semi-solid network that encapsulates the biochar particles and magnetic material.[70] Another important process that occurs is *in situ* cross-linking, in which a solution containing gel precursor is mixed with calcium chloride for alginate that induces the gel to form immediately, binding the components together into a bead-like structure.[71,72] On the other hand, calcination involves the thermal treatment where the gelated materials are heated at high temperatures, which serves to harden the gel, remove the volatile compounds, and decompose the biochar, enhancing the adsorptive properties.[73,74] Furthermore, calcination involves the incorporation of metal ions into a biochar matrix to improve the magnetic properties of beads. Specifically, the gelation process involves the cross-linking of biochar with lanthanum alginate to form beads, while calcination plays an important role in stabilizing the beads and incorporating magnetic materials that enhance the removal of contaminants.[75,76] Overall, gelation–calcination is widely utilized technique for the development of adsorbent beads with tailored surface properties, defined morphology, and magnetic functionality for wastewater treatment. Several studies have utilized the gelation–calcination process to prepare magnetic beads. For instance, Wang *et al.* prepared lanthanum alginate beads incorporated with $MgFe_2O_4$-biochar for efficient phosphate ion removal. In this study, the authors utilized a gelation–calcination approach using Mg/Fe, BM, and Mg/Fe–BM precursors to prepare slurries, which were subsequently heat-treated at different temperatures in a nitrogen-purged muffle furnace. The study developed BM–La(b), $MgFe_2O_4$–La(b), and $MgFe_2O_4$–BM–La(b), which were recognized for their ability to remove phosphate ions.[77] In another instance, Wei *et al.* focused on the preparation of $MgFe_2O_4$-doped biochar beads for removing Sb(v) ions. The study illustrates the gelation–spheroidization–carbonization process for the synthesis of biochar beads.[78] In summary, the gelation–calcination process was found to be efficient for the preparation of biochar-based magnetic beads with controlled surface characteristics, morphology, and improved adsorption and magnetic performance. Notably, the calcination is basically a heating process for optimizing the roughness of the surface, which is usually a challenging part for the effective removal of environmental contaminants.

3. Applications of biochar-based beads for wastewater treatment

Biochar-based bead adsorbents have demonstrated their versatility in addressing various kinds of pollutants, including dyes, heavy metals, pharmaceutical pollutants, and nutrients, by integrating biochar with polymers, clays, and magnetic materials. Owing to their unique surface properties, ease of recovery, and cost-effectiveness, biochar-based composite beads have gained increasing interest in research for the effective removal of pollutants using different techniques. A comprehensive summary of recent studies investigating biochar-based bead composites for the removal of pollutants, their compositions, removal capacities, and synthesis methods is illustrated in Table 1. For instance, Zou *et al.* developed FCB beads and FCH beads utilizing coffee grounds as a natural precursor. In this study, the authors utilized radical and non-radical pathways for the degradation of oxytetracycline hydrochloride (OTC). This process involves several reactions during the study, including ring-opening reactions, demethylation, and hydroxylation.[79] The study observed that oxygen-containing species in the adsorbent contribute to the removal of OTC *via* the quenching mechanism. The key finding of the study suggests the combined action of radicals and nonradical pathways for the elimination of OTC. The preparation of beads during pyrolysis increases the generation of oxygen-containing reactive species, showing the Fenton-like reactions through the abundance of functional groups. In another study, Das *et al.* developed CA–B/ABC beads for the removal of MB with the

Table 1 Comparative analysis of biochar-based bead adsorbent for wastewater remediation, highlighting adsorbent composition, targeted pollutants, natural precursor, operational pH, mechanism involved, and technique utilized in previous studies

S/N	Pollutant	Adsorbent/material	Adsorption capacity ($mg\ g^{-1}$)	Natural precursor	pH	Mechanism	Technique	Ref.
1	Levofloxacin	Chitosan/poly(vinyl alcohol)-biochar@Co–Ni–Al LDH	1795.007 $mg\ g^{-1}$	*Hydrocotyle vulgaris* (HV)	8.5	H-bonding, anion exchange, electrostatic, complexation, and π–π stacking	Ionotropic gelation technique	89
2	Methylene blue	BCA-Mag/AB	23.99 $mg\ g^{-1}$	Pomegranate peel	6	Hydrophobic, electrostatic and π–π stacking	Physical crosslinking methods	90
3	Phosphate	SA-KBC-Fe/La beads	46.65 $mg\ g^{-1}$	Sludge	6	Ligand exchange and electrostatic attraction	Sol–gel	91
4	Chlorpyrifos pesticide	Sugarcane bagasse-based BAB	91.93 $mg\ g^{-1}$	Sugarcane bagasse	6	Electrostatic interactions and π–π electron interactions	Ionotropic gelation technique	84
5	Cr(VI)	EC-Alg/PEI-3	769.2 $mg\ g^{-1}$	*Eichhornia crassipes*	2.4	Electrostatic attraction, pore-diffusion, complexation	Ionotropic gelation combined with PEI functionalization	92
6	Methylene blue	BC/Alg composite	9.67 $mg\ g^{-1}$	Argan nutshells	8	π–π interactions	Ionotropic gelation	93
7	Phosphorus	Modified biochar beads	253.88 $mg\ g^{-1}$	*Hydrocotyle vulgaris*	—	Pore-filling, hydrogen bonding, surface complexation	Ionotropic gelation	86
8	Methylene blue	Activated biochar/polyaniline/alginate composite beads (ABC–PA–SG)	821 $mg\ g^{-1}$	*Crataegus azarolus* seed waste	6.4	Pore filling, π–π interactions	Encapsulation/gelation	87
9	Ammonia nitrogen, phosphorus, organic carbon, copper, and zinc	Biochar-Chlorella pyrenoidosa beads	—	*Chlorella pyrenoidosa*	7	Ion-exchange, metal-coordination	Pyrolysis	69
10	Ciprofloxacin	Chitosan/biochar hydrogel beads	36.72 $mg\ g^{-1}$	Pomelo peels	3	H-bonding, EDA, hydrophobic interactions	Pyrolysis	94
11	Cd(II)	Ca-alginate ball-milled biochar beads	227.1 $mg\ g^{-1}$	Bamboo	5	Ion-exchange	Ball-milled	88
12	Phosphate	Sludge-based magnetic gel bead	87.79 $mg\ g^{-1}$	Sludge	5.13	Surface precipitation and Fe–O–P bonding	Macro–micro hybrid	95
13	Methylene blue (MB)	Fe_3O_4-modified coconut shells biochar (mCSB)/sodium alginate (SA) aerogel bead	124.0 $mg\ g^{-1}$	Coconut shells	7	Pore-filling, electrostatic attraction, hydrogen bond interaction	*In situ* crosslinking-gelation method	54
14	Ciprofloxacin	SA/H_3PO_4-activated CC-ABC	97.10 $mg\ g^{-1}$	Corncob	6	H-bonding, π–π, electrostatic interaction	Facile phase inversion method	96
15	Phosphate	$MgFe_2O_4$-biochar based lanthanum alginate beads	23.76 $mg\ g^{-1}$	*Phragmites australis*	5.3	Inner-sphere complexation and ligand-exchange	Gelation *via in situ* crosslinking	77
16	Copper ions	Magnetic-biochar/alginate bead	234.06 $mg\ g^{-1}$	Peanut shells	5	Complexation, pore-filling, ion exchange, van der Waals force	Physical cross-linking	82

Table 1 (*Contd.*)

S/N	Pollutant	Adsorbent/material	Adsorption capacity ($mg\ g^{-1}$)	Natural precursor	pH	Mechanism	Technique	Ref.
17	Oxytetracycline hydrochloride	Ferric crosslinked alginate materials-biochar beads (FCB beads) and hydrogel beads (FCH beads)	—	Coffee grounds	4.5	Radical and non-radical pathways	Cross linking-gelation method	79
18	Methylene blue	Calcium alginate–bentonite/activated biochar composite beads	47.393 $mg\ g^{-1}$	Sugarcane bagasse	5.7	Complexation, chemical interaction	Chemical-activation	80
19	Phosphate	Magnesium-modified biochar beads	53.2 $mg\ g^{-1}$	Maize straw	4	Electrostatic interactions, and precipitation	Ball milling	81
20	Sulfathiazole	Magnetic chitosan–BC–Fe microsphere beads	98.67 $mg\ g^{-1}$	*Conocarpus* waste	5	Pi–pi electron-donor–acceptor interactions and Lewis acid–base reactions	Pyrolysis	83
21	Sb(v)	Magnetic $MgFe_2O_4$–2 biochar composite beads	125.65 $mg\ g^{-1}$	Waste reeds	5.5	Ligand exchange, inner-sphere complexation, H-bonding	Co-precipitation method	78
23	Organic matter (humic acid)	Magnetic biochar-iron cross-linking alginate (MBCA) beads	—	Coffee grounds	—	Radical oxidation and coagulation	Gel-pyrolysis	66

maximum adsorption capacity of 47.393 $mg\ g^{-1}$.[80] Likewise, for the removal of nutrients, Hu *et al.* explored the magnesium-modified biochar beads which showed high potential towards the removal of phosphate. This work utilized the ball milling technique to functionalize the biochar with metal oxides, using $MgCl_2 \cdot 6H_2O$ as a precursor. Additionally, biochar beads were made from sodium alginate and Fe_3O_4, which have a high adsorption ability for phosphate removal, with a value of 53.2 $mg\ g^{-1}$. The large surface area, oxygen-containing functional groups, and reduced particle size all help with adsorption.[81] The adsorption capacity of bare biochar is ~3.2 $mg\ g^{-1}$, while magnesium-modified biochar beads have an adsorption capacity of 53.2 $mg\ g^{-1}$ for phosphate (PO_4–P). Furthermore, shifting the focus to heavy metal pollutants, Ben Salem *et al.* investigated magnetic-biochar/alginate beads that demonstrate their strong ability for the adsorption of Cu^{2+} ions. The prepared beads achieved the maximum adsorption capacity of 234.06 $mg\ g^{-1}$, which was derived using peanut shells by the cross-linking process. The study states that the interaction occurs between the functional groups present on the surface of the bead and Cu^{2+} ions through physical adsorption.[82] This occurs due to the solution pH being 5, where the surface was positively charged and interacts with negatively charged metal ions *via* electrostatic interactions. The study indicates that complexation, van der Waals forces, and ion exchange were the main mechanisms followed during the adsorption of toxic Cu^{2+} ions. The combination of biochar, magnesium ferrite, and sodium alginate enhances the performance of the material, improving its separation efficiency and making it more effective for the removal of pollutants. This combination also enhances the adsorption efficacy of biochar.[78] Moreover, to enhance the magnetic functionality, Wei *et al.* developed $MgFe_2O_4$-doped biochar beads through a gelation–spheroidization–carbonization process. To evaluate the changes in the adsorption capacity of antimony using composite beads, different adsorbents with modified materials were tested. In addition, pristine biochar along with MgFeO, MgFeO–BC, Fe–BC, and Fe/(MgFeO–BC) were examined for their adsorption ability to adsorb antimony. The study reveals that pristine biochar and MgFeO show a somewhat negligible adsorption effect, while the adsorption capacity of Fe/BC is also limited. Moreover, the inclusion of $MgFe_2O_4$ plays a significant role in serving as an active adsorption centre within the beads. Also, the formation of sphere structures enhances the performance of Fe/(MgFeO–BC), which promotes the dispersion of NPs. However, pre-experiments in the study show a synergistic effect between MgFeO, biochar, and the bead structure in Fe/(MgFeO–BC) adsorption capacity. Owing to this, the study shows that Fe and Mg proportions remain constant throughout the adsorption process, which makes the material's stability constant. The Sb element is adsorbed indicating the Fe and Mg elements are involved in the adsorption process. Furthermore, $MgFe_2O_4$ plays a key role with superparamagnetic properties in the adsorption of Sb, acting as a binding site for adsorption, which is due to its surface properties, which exhibits interactions with Sb molecules. The study reveals that the adsorption of $Sb(OH)_6^-$ on Fe/(MgFeO–BC) takes 400 minutes, which is significantly longer compared to the

adsorption on the composite bead. In contrast, the composite bead exhibited extremely high adsorption, with 80% removal of $Sb(OH)_6^-$ within just 45 minutes. The study shows that after 350 minutes, equilibrium was reached, and no further adsorption occurred. The highest adsorption rate of Fe/(MgFeO–BC) towards $Sb(OH)_6^-$ facilitates synergistic adsorption effect.[78] Also, Al-Wabel *et al.* synthesized chitosan–biochar beads derived from *Conocarpus* for the efficient removal of sulfathiazole for wastewater treatment.[83] Likewise, Fan *et al.* investigated the coconut shell-derived biochar-based sodium alginate composite for the adsorption of methylene blue. The authors prepared Fe_3O_4-modified coconut shell biochar using a cross-linking-gelation process.[54] In addition, Jacob *et al.* prepared biochar–alginate beads utilizing sugarcane bagasse as the feedstock for the adsorption of chlorpyrifos. The prepared beads show high potential for the removal of chlorpyrifos with contributing high surface area of 131.09 $m^2\ g^{-1}$ and a pore volume of 0.165 $cm^3\ g^{-1}$. The study revealed that enhancement in biochar surface and pore volume is attributed to the incorporation of sodium alginate, which enhances the density of functional groups and structural stability confirmed using SEM analysis.[84] To explore the thermal modification techniques, Kang *et al.* developed calcined alginate beads using alum sludge to enhance the adsorption of arsenic (As) ions. In this study, adsorbent beads were prepared using the calcination process of polyvinyl alcohol and sodium alginate in powder form. The adsorption capacity of the calcination process decreases compared to the un-calcined adsorbent.[85] Also, Fu *et al.* prepared biochar beads using *Hydrocotyle vulgaris* to enhance the recovery rate of phosphorus. The prepared adsorbent reveals a surface area of 266.423 $m^2\ g^{-1}$ with a pore size of 9.216 nm, resulting in better adsorption. In the initial time of 160 minutes, the adsorption was completed. During the starting stage, adsorption was rapid and then reached equilibrium. The initial concentration of MBCB was increased to enhance the diffusion rate and hence the adsorption rate.[86] The ΔH values indicate that the reaction was endothermic and showed the hydrogen bonding, van der Waals force, and dipole interactions. The initial concentration of MBCB was increased from 5 $mg\ L^{-1}$ to 15 $mg\ L^{-1}$. As a result, the infiltration curve also increased, while both the infiltration time and saturation time were shortened. This increase in concentration enhances the acceleration and internal driving force while reducing the contact time between adsorbents and adsorbates. Also, Faouzia *et al.* investigate the morphology of ABC–PA–SG using SEM analysis, which reveals the surface before and after adsorption of methylene blue. The study indicates that the surface of the prepared adsorbent has many holes, which are useful for better adsorption.[87] The change in surface morphology was observed in which the surface became smooth after adsorption, indicating that methylene blue molecules were successfully adsorbed onto the surface.

The study reported by Wang *et al.* follows the Langmuir equation to explain the adsorption of prepared sorbents over the Freundlich equation. In this study, the interaction between Cd(II) ions and the prepared adsorbent was mainly due to the occurrence of oxygen-containing species on the adsorbent surface. The larger the availability of functional groups on the adsorbent surface, the higher the active sites. The mixture of calcium alginate and biochar-based beads improves the adsorption potential of CA-BMB.[88] Furthermore, Li *et al.* investigated the use of magnetic biochar beads, pretreated with peroxymonosulfate, to prevent membrane clogging in the ultrafiltration process. In this study, the authors utilized magnetic biochar-iron cross-linked alginate beads (MBCA) made from coffee grounds as a natural precursor. The study explains the adsorption mechanism of MBCA beads, where pollutants are adsorbed through H-bonding, electrostatic interactions, and chemical and physical forces.[66] These processes generate radicals *via* different pathways. The study focuses on radical oxidation and coagulation for the removal of humic acid and sodium alginate, with hydroxyl radicals playing a significant role in the process. The survey of previous studies shows that to further improve the selectivity, stability, and multi-contaminant removal capabilities of biochar-based composite beads, more research in this area is required. Despite the promising results of these composites, more research is needed to optimize synthesis methods and to understand their long-term impact on the environment. To better understand the effectiveness of biochar-based bead composites, the next section explores fundamental mechanisms that govern their enhanced adsorption performance against various pollutants.

3.1 Mechanism of biochar-based beads in water treatment

Biochar-based beads have demonstrated promising results in the adsorption/removal of various contaminants from water. The mechanisms involved during the adsorption process are electrostatic forces, hydrogen bonding, and π–π stacking, as well as ligand exchange and redox reactions. Based on the previous experimental evidence, this section categorizes and discusses these mechanisms in detail. Moreover, a clear understanding of these interactions is crucial for optimizing the performance of biochar-based bead adsorbents in real-world water treatment applications.

3.1.1 Electrostatic interactions. Electrostatic attraction plays a major role in the adsorption of charged contaminants onto biochar-based beads.[97] For instance, the study by Fan *et al.* reported that the adsorption mechanism through four steps: (i) diffusion of methylene blue on aerogel beads, (ii) intra-particle diffusion, (iii) filling of active sites, and (iv) electrostatic interaction. The study demonstrated electrostatic interaction was the dominant mechanism during MB dye adsorption onto mCSB/SA aerogel beads, as shown in Fig. 2b. Additionally, the incorporation of SA into the composite introduced more hydroxyl-like groups on the bead surface that form hydrogen bonds with N^+ groups, thereby increasing adsorption efficacy. The enhancement in adsorption capacity from 65.27 $mg\ g^{-1}$ to 124.0 $mg\ g^{-1}$ was ascribed to the synergistic effect of functional groups and a highly porous structure.[54] In another study, Jacob *et al.* suggested that hydroxyl groups on the biochar surface attract the phosphate group of chlorpyrifos following electrostatic interaction. The adsorption of CPS was followed the

Yoon–Nelson kinetic model, indicating availability of active sites enhances the adsorption performance. Moreover, the dominant adsorption mechanism involves electrostatic interactions, π–π stacking, and hydrogen bonding.[84] In addition, π–π interactions occur between the aromatic, carbon-rich surface of biochar, while hydrogen bonding occurs between hydrogen atoms on the biochar surface and negatively charged phosphate groups of CPS.

3.1.2 π–π electron donor–acceptor interactions. The π–π stacking is a key mechanism involves during the adsorption of aromatic compounds. Various studies have demonstrated the interaction of aromatic ring structures in dyes with graphitic domains of biochar-based adsorbent *via* π–π donor–acceptor mechanisms. The study by Al-Wabel *et al.* demonstrates that STZ adsorption follows multiple mechanisms, including electrostatic interactions, H-bonding, and π–π EDA interactions. At below pH 3, the STZ behaves as a cation, and between pH 3 and 6, it acts as an anion. The study reveals the highest removal of STZ at pH 5, and at pH > 6, the adsorption decreases due to repulsions between the negatively charged adsorbent and the negatively charged STZ. This indicates that electrostatic repulsions were not the dominant removal mechanism during the study. When the pH of the solution exceeds 6, lewis acid–base reactions and π–π EDA interactions become the dominant mechanisms for STZ removal. The amino and sulfonamide groups of STZ interact with the hydroxyl groups of the adsorbents through Lewis acid–base reactions.[83] Under acidic conditions, STZ acts as a π electron acceptors, which promote the π–π EDA interactions and thus enhance the removal of STZ. Compared to BC and CBC, the highest adsorption capacity was observed in CBC–Fe, attributed to its high surface area, more surface functional groups, and strong magnetic properties. The study shows that the main adsorption mechanisms followed during the study are pore diffusion, hydrogen bonding, Lewis acid–base reactions, and π–π EDA interactions. The rate of adsorption was higher initially, likely due to the presence of more available active sorption sites. However, with the occupancy of active sites, their activity decreased, and equilibrium was eventually reached. As per the study, the adsorption capacity of STZ reached 75.84 mg g^{-1} with CBC–Fe, whereas CBC and BC exhibited lower values of 42.73 mg g^{-1} and 34.05 mg g^{-1}, respectively. The adsorption capacity increases with the number of functional groups and the higher surface area of CBC–Fe. The rate of adsorption was higher initially, likely due to the presence of more available active sorption sites. The higher efficiency of CBC–Fe for STZ is mainly due to highly conducting microsphere beads, which degrade the STZ molecule through the generation of $HO^{\bullet}$ radicals. Also, the study by Faouzia *et al.* reveals that the π–π stacking mechanism plays a major role in explaining the adsorption phenomenon of methylene blue. Moreover, electrostatic attractions take place between the negatively charged oxygen-containing groups and cationic dye molecules. The study also found that the H-bonding between the acidic protons and the nitrogen atoms of methylene blue molecules enhances the binding affinity, as shown in Fig. 1b. The synergistic interactions that occur between the biochar/polyaniline/alginate composite beads facilitate a higher adsorption capacity over bare substrates.[87] The study by Küçük *et al.* prepared biochar with magnetite and alginate beads using orange peel as a natural precursor for the adsorption of methylene blue. The surface area and pore volume of the prepared adsorbent were found to be 455.4 m^2 g^{-1} and 0.268 cm^3 g^{-1}, respectively. The optimal conditions that resulted in maximum removal of methylene blue (MB), achieving 98% removal efficiency using BCA-Mag/AB dosage of 0.10 g/50 mL in 150 minutes.[90]. The synthesized BCA-Mag/AB

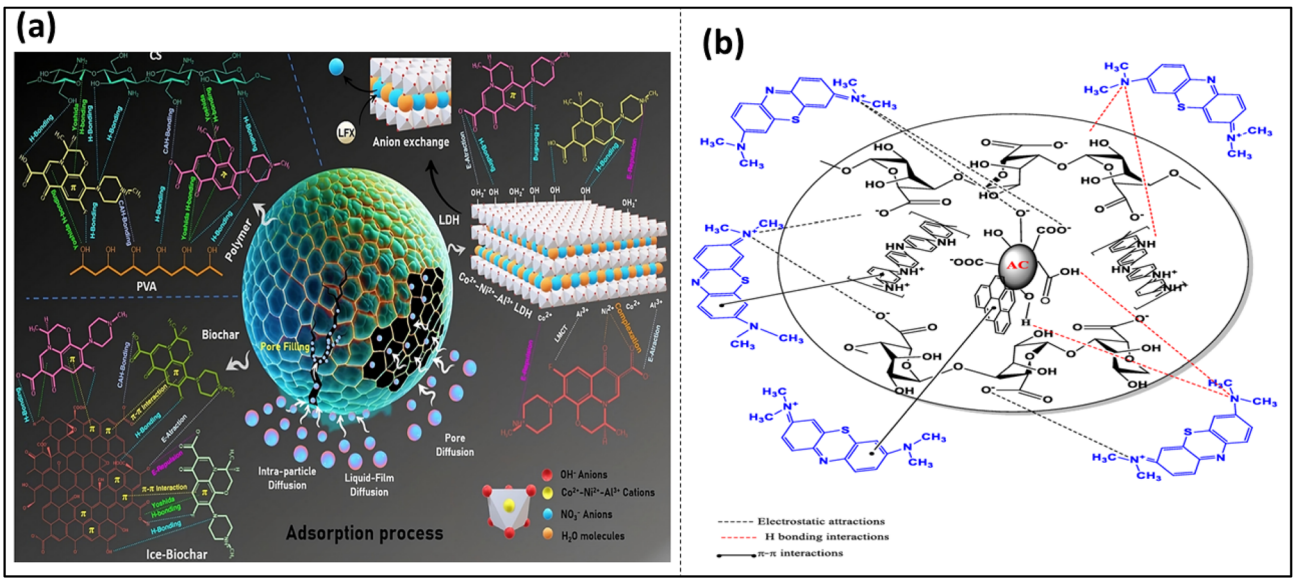

Fig. 1 (a) Schematic illustration of the adsorption mechanism of levofloxacin onto LDH–BC/CS–PVA beads. This figure has been reproduced from ref. 89 with permission from Elsevier, copyright 2025. (b) Mechanistic representation of the adsorption of methylene blue using biochar/polyaniline/alginate composite beads. This figure has been reproduced from ref. 87 with permission from Elsevier, copyright 2025.

adsorbent was found to contain variety of functional groups which are associated with alcohols, phenols, or ethers. The synergistic interactions play main role during the adsorption of MB dye using m-(BCA-Mag/AB) adsorbent. Also, Mosaffa *et al.* utilized *Hydrocotyle vulgaris* (HV) as a biomass for the preparation of CS/PVA–biochar@Co–Ni–Al LDH beads with a surface area of 176.21 $m^2\ g^{-1}$. This was prepared by incorporating layered-double hydroxide-modified biochar with polyvinyl alcohol and chitosan matrix. For levofloxacin removal, the adsorption mechanism was attributed to synergistic interactions of complexation, anion exchange, H-bonding, and π–π interactions[89]. Furthermore, the porosity of the beads increases due to the occurrence of hydrogen bonds of PVA with LDH hydroxide groups, which simultaneously improves the cross-linking between LDH particles and polymer matrix. The mechanistic representation of adsorption of levofloxacin on LDH–BC/CS–PVA beads has been demonstrated in Fig. 1a.

3.1.3 Hydrogen bonding. Hydrogen bonding is frequently involved in the adsorption of organic contaminants. For instance, the study by Bahsaine *et al.* investigated the preparation of biochar–alginate beads derived from argan nutshells for the effective removal of methylene blue. The study performed the adsorption process using 120 mg L^{-1} of methylene blue concentration with the pH of 8, contact time of 50 minutes, under which the maximum adsorption efficacy of 96.4% was achieved. Moreover, the temperature of the process highly influences the adsorption efficiency of MB, as at low temperatures, the adsorption capacity was also low, and *vice versa*. The adsorption of methylene blue onto BC/Alg composite beads involved multiple mechanisms, including hydrogen bonding, pore diffusion, electrostatic attraction, and π–π interactions.[93] These interactions are influenced by the type of functional groups and surface electrical properties. The study found that π–π stacking plays the main role due to the interaction between the graphitic carbon domains of biochar and the aromatic rings of MB. The XRD analysis has shown that biochar can act as π–electron donors, and on the other hand, methylene blue has positively charged cationic nitrogen that acts as π–electron acceptors. This synergistic effect facilitates strong π–π and π^+–π interactions. Additionally, hydrogen bonding between MB molecules and oxygen-containing functional groups on the adsorbent surface contributes to an increase in adsorption efficiency. These interactions contribute to the strong affinity of BC/Alg composites towards MB removal.

3.1.4 Ligand exchange and complexation. Ligand exchange and metal complexation are dominant mechanisms in the removal of heavy metals. For instance, He *et al.*, prepared biochar skeletal sodium alginate beads using municipal sludge as a natural precursor for the removal of phosphate. The SA-KBC-Fe/La composite was synthesized *via* sol–gel method, which exhibits a 46.65 mg per g phosphate uptake capacity. The adsorption mechanism of sludge-derived biochar alginate beads doped with iron and lanthanum (SA-KBC-Fe/La) is performed at optimal pH 6 with the surface area of 54.22 $m^2\ g^{-1}$, and was found to involve ligand exchange, electrostatic attraction, and H-bonding. The ligand exchange mechanism involves oxygen-rich phosphate species that form inner-sphere complexes with Fe and La atoms by replacing surface hydroxyl groups, resulting in the formation of stable Fe–O–P and La–O–P bonds. Additionally, electrostatic attraction is facilitated by the formation of $La–OH_2^+$ on the adsorbent surface, which attracts negatively charged phosphate ions to form outer-sphere complexes.[91] These findings suggest that phosphate adsorption occurs through a synergistic combination of physical and chemical mechanisms, including electrostatic interaction, hydrogen bonding, and strong chemisorption through ligand exchange, thereby contributing to the enhanced removal efficiency of the composite beads. Also, the occupancy of functional groups significantly enhances the formation of active adsorption sites, as reported by Wei *et al.* The study found that the adsorption mechanism involves multiple steps, including surface protonation, electrostatic interaction, ligand exchange, and hydrogen bonding. Initially, surface hydroxyl groups undergo protonation:[78]

$$\text{Protonation: bead–M–OH} + H^+ \rightarrow \text{bead–M–}OH_2^+$$

$$\text{Electrostatic attraction: bead–M–}OH_2^+ + Sb(OH)_6^- \rightarrow \text{bead–M–}OH_2^+\cdots Sb(OH)_6^-$$

$$\text{Ligand exchange/inner-sphere complexation: bead–M–OH} + Sb(OH)_6^- \rightarrow \text{bead–M–O–}Sb(OH)_5^- + H_2O$$

$$\text{Bead–M–}OH_2^+ + Sb(OH)_6^- \rightarrow \text{bead–M–O–}Sb(OH)_5^- + H_3O^+$$

$$\text{Hydrogen bonding: bead–M–OH}\cdots Sb(OH)_6^-$$

3.1.5 Redox reactions. Redox interactions are essential in adsorbing redox-active pollutants such as hexavalent chromium (Cr^{6+}). For instance, Faouzia *et al.* demonstrated that Fe^{3+} sites in alginate–chitosan–biochar beads acted as reducing agents, converting Cr^{6+} to Cr^{3+}, which is then adsorbed onto the bead surface. This dual mechanism of reduction followed by complexation significantly increased Cr^{6+} removal efficiency.[87] In another study, He *et al.* developed AFB/Alg beads with polyethyleneine (PEI) modifier to achieve the improvement in removal rate of Cr(VI) ions. Thereby, maximum adsorption capacities of EC-alg/PEI-3 were noted as 714.3 mg g^{-1} at 10 °C and 769.2 mg g^{-1} at 25 °C. The authors evaluates at low pH values, electrostatic interactions play main role where amino groups present on the bead surface gain protons and become positively charged.[92] Simultaneously, Cr(VI) exists in its negatively charged $HCrO_4^-$ or $Cr_2O_7^{2-}$ forms, which are attracted to the positively charged adsorbent surface. The electrostatic interaction can be represented as:

$$–NH_3^+ + HCrO_4^- \rightarrow –NH_3^+\cdots HCrO_4^-$$

At lower pH values, Cr(VI) is reduced to its more stable form, Cr(III). The redox reactions are facilitated by hydroxyl and amino groups present on the adsorbent surface which act as electron donors to Cr(VI). The redox reaction involved in this study are as follows:

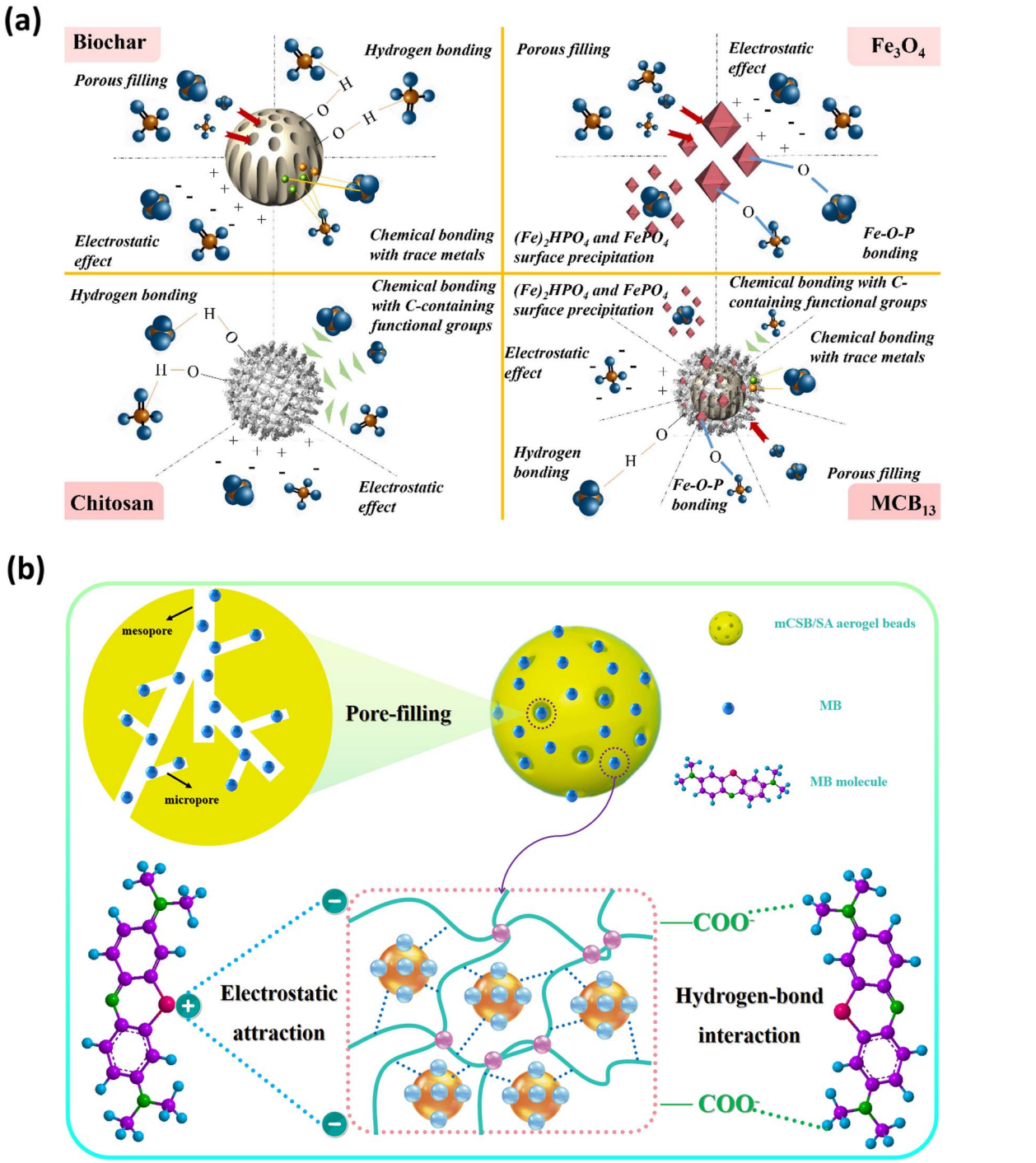

Fig. 2 (a) Mechanistic representation of phosphate removal by biochar, chitosan, Fe_3O_4, and MCB_{13}. This figure has been reproduced from ref. 95 with permission from Elsevier, copyright 2021. (b) Adsorption of MB molecules on the surface of mCSB/SA aerogel beads. This figure has been reproduced from ref. 54 with permission from Elsevier, copyright 2025.

$$HCrO_4^- + 3e^- + 7H^+ \rightarrow Cr^{3+} + 4H_2O$$

$$Cr_2O_7^{2-} + 6e^- + 14H^+ \rightarrow 2Cr^{3+} + 7H_2O$$

After the formation of Cr(III), it sticks on the adsorbent surface *via* coordinate interactions with the amino groups.

$$R\text{–}NH_2 + Cr^{3+} \rightarrow R\text{–}NH_2 \rightarrow Cr^{3+}$$

Therefore, the removal of Cr(VI) using EC-alg/PEI-3 beads is governed by a synergistic combination of electrostatic attraction, redox transformation, and subsequent chelation with functional groups on the adsorbent surface.

3.1.6 Pore filling and physical adsorption. Pore filling is one of the key mechanisms that play a crucial role in the adsorption efficiency of biochar-based beads. The effective adsorption of contaminants requires a highly porous structure of adsorbent, owing to its large surface area and active adsorption sites. For instance, Li *et al.*, investigated the sludge-based biochar beads for the adsorption of phosphate ions. The study shows that the porous structure of biochar plays a vital role in adsorption. The study observed the porosity of biochar with and without N_2 gas, and it was noted that in the presence of N_2 gas, biochar exhibited a highly porous volume. Due to the low affinity of biochar towards the phosphate ion, it fails to adsorb significant amounts of phosphorus molecules.[95] In contrast, MCB_{13} and Fe_3O_4 exhibit enhanced adsorption performance after loading with phosphorus ions. The mechanistic representation of phosphate removal by biochar, chitosan, Fe_3O_4, and MCB_{13} is shown in Fig. 2a. After some time, a decrease in surface area, total pore volume, and mesopore volume is observed due to the pore occupation by phosphorus molecules. In another study, the primary absorption mechanism follows monolayer chemisorption, dominated by strong ionic and covalent bonds. Electrostatic interactions, hydrogen bonding, ion-exchange, complexation, and π–π stacking interactions are the key mechanisms involved during the study. At solution pH below 8.4, the adsorbent surface acquires positive charge, mainly due to the protonation of hydroxyl and carboxyl groups. The anionic LFX species and positively charged species follow electrostatic interactions. Hydrogen bonding occurs between biochar, LDH, $–NH_2$ (from chitosan), and heteroatoms in LFX (–COOH, F, $–NR_2$). These synergistic interactions enable high adsorption capacity and selectivity for LFX.[89]

3.2 Experimental parameters

This section discusses the impact of optimization of different experimental parameters on the adsorption performance of the prepared adsorbents.

3.2.1 pH. The pH of the solution is one of the most important parameters that affects the adsorption efficiency of biochar-based beads. It significantly alters both the surface charge of the adsorbent and the speciation of the target contaminants. At low pH values, a large number of H^+ ions are released into the solution that compete with the positively charged methylene blue molecules for the availability of active adsorption sites. The increased concentration of H^+ ions can displace the methylene blue molecules from the surface of the adsorbent. However, at high pH values, the concentration of hydroxide ions increases, which deprotonates the functional groups. The positively charged methylene blue molecules bind through the electrostatic force of attraction with the negatively charged surface functional groups. The study by Fan *et al.* observed that with an increase in pH value, adsorption capacity increases, reaching 124.0 mg g^{-1} at a pH 7.[54] Moreover, the pH of the solution highly influences the adsorption potential of the prepared composite. The study reveals that when solution pH exceeds, the surface of the adsorbent becomes negatively charged which facilitates more attraction of methylene blue cations. On the other side, at low pH values, the surface becomes positively charged which repels the methylene blue molecules and decreases the adsorption capacity. Furthermore, with a rise in pH, the adsorption of MB increases because the hydroxide ion deprotonates the NH_2^+ groups, which create more negative sites that attract more cationic methylene blue. The prepared composite ABC–PA–SG had acidic pH_{pzc} because polyamine contains more positively charged groups.[87] The study by Mosaffa *et al.* showed that varying the pH from 4–10 affects the adsorption rate. The maximum adsorption was achieved using 5 mg of prepared adsorbent and 20 mL of 100 mg L^{-1} levofloxacin solution at a pH of 8.5. The increase in pH up to a certain limit also increases the availability of $–NH_2$ and –OH functional groups on the adsorbent surface, which helps to improve adsorption performance. However, the authors confirmed that with further rise in pH values, decreases in adsorption performance were found, which happens due to surface characteristics of the beads being altered.[89] Additionally, the study describes the adsorption performance of the prepared adsorbent at different pH values. Initially, pH increases from acidic (5.59) to neutral value (7.94), it undergoes

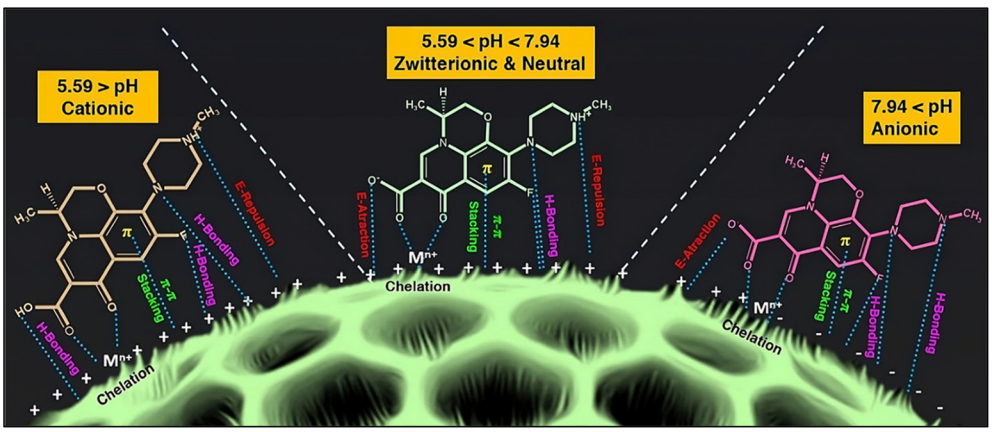

Fig. 3 Structural forms of LFX at different pH levels and their possible interactions with the adsorbent. This figure has been reproduced from ref. 89 with permission from Elsevier, copyright 2025.

deprotonation, forming a zwitterionic structure. The electrostatic attraction occurs between the negatively charged carboxylate groups and the positively charged adsorbent surface. Above pH 7.94, deprotonation of the tertiary amine group of LFX molecules producing the anionic form of molecules. At the end stage, up to $pH_{pzc} \approx 8.4$, the adsorbent surface gets positively charged, which facilitates electrostatic attraction, hydrogen bonding, and chelation. However, when pH exceeds 8.5, removal efficiency starts decreasing because of the repulsion between the negatively charged adsorbent surface and anionic LFX.[89] The different structural forms of LFX at different pH levels and their possible interactions with the adsorbent have been shown in Fig. 3. In another study, He *et al.* examined the pH effect on the adsorption of Cr(VI) by varying the pH values of the solution. In contrast to this, Cr(VI) behaves differently in different pH conditions as per the applicability of the types of interaction at that pH value. The study revealed that adsorbents show a reduction in adsorption capacity with an increase in pH value due to the ionic size of CrO_4^{2-}. Furthermore, different forms of Cr(VI) under varying pH values are categorized into (i) H_2CrO_4, at pH < 2; (ii)$HCrO_4^-$, between pH 2–3; (iii) CrO_4^{2-}, when pH > 6.8. Among these, $HCrO_4^-$ is the predominant form for Cr(VI) adsorption; it adsorbs easily in solution, and facilitates better adsorption. Therefore, the maximum adsorption capacity, reaching 350.5 mg g^{-1}, was observed at pH 2. When pH exceeds 6.8, competitive adsorption between hydroxyl ions and the larger ionic radius of CrO_4^{2-} hinders Cr(VI) removal efficiency.[92] This was explained based on the fact that at lower pH values, various positively charged species are present, which reduces from Cr(VI) to Cr(III). The study by He *et al.* found that the adsorbent surface contains carboxyl and amino groups, making the adsorbent surface positively charged. In contrast, the H^+ ions start decreasing with an increase in pH, resulting in decline in Cr(VI) adsorption efficiency. Likewise, the solution pH plays significant role in governing the adsorption potential of phosphate using the SA-KBC-Fe/La composite. At pH 2, adsorption capacity was 21.37% at pH 2 which rises with an increase in pH and reached a maximum at pH 6. With a further increase in pH from 7 to 11, the removal rate decreases. The maximum adsorption capacity, 46.65 mg g^{-1}, was achieved at pH 6. When the pH < 2, the adsorbent surface carries a positive charge which contains H_3PO_4 and $H_2PO_4^-$, with H_3PO_4 having almost no contribution to adsorption. From the pH range of 2–12, $H_2PO_4^-$ and HPO_4^{2-} are the dominant phosphate species. However, at pH > 8, the deprotonation of functional groups competes with phosphate for active species, which reduces the electrostatic attraction and leads to a decline in adsorption efficiency.[91]

$$PO_4^{3-} + H_2O \rightleftharpoons HPO_4^{2-} + OH^-$$

$$HPO_4^{2-} + H_2O \rightleftharpoons H_2PO_4^- + OH^-$$

$$H_2PO_4^- + H_2O \rightleftharpoons H_3PO_4 + OH^-$$

The pH is a critical parameter since it influences the chemical stability of both the adsorbent materials and metal ions. For instance, Ben Salem *et al.* evaluated the wide range of pH values to find out the optimum pH value for maximum removal efficiency. In acidic conditions, electrostatic repulsion occurs, caused by competing ions. Conversely, at higher pH values, the surface gets negatively charged, which binds the positively charged metal ions, thereby affecting the adsorption efficiency. The study shows that the optimal pH value selected for the study is 5, and surface complexation and chelation occur due to density of functional groups.[82] Several studies observed the same trend, an increasing adsorption efficiency with rising pH. Also, Zou *et al.*, reported decrease in adsorption rate was observed at a pH value 3 decreased due to highly acidic medium. The removal efficiency of oxytetracycline hydrochloride at pH value 3 decreased due to the presence of competing ions and electrostatic repulsion between the positively charged metal ions and the surface of beads. At a pH value of 3, the removal efficiency starts increasing from 90.34%, and at pH of 4.5, the highest removal rate of 91.24% was observed for FCB beads/H_2O_2 and 91.31 for FCH beads/H_2O_2 respectively. When the pH was further increased, a decrease in removal rate was observed due to the formation of the complex. The solution pH is a main parameter that affects the adsorption of pollutants by dissociation of functional groups on the adsorbent surface.[79] Also, Das *et al.*, optimize the variation in pH from 2–8 with constant adsorbent dosage and concentration of methylene blue. At higher pH value, the adsorbent surface becomes negative and the molecules of methylene blue are positively charged which attracts each other enhances the adsorption capacity. In contrast at low pH values, the molecules of methylene blue dissociates into negatively charged which attracts positive charge species on the surface of adsorbent.[80] Due to electronegative charge density on biosorbent, the adsorption is higher on high pH values rather than at low pH values. Also, Hu *et al.* observed the effect of solution pH on adsorption efficacy, noting that low pH values decreased adsorption due to electrostatic repulsions. At pH 4, the surface of the beads is negatively charged, and the binding between the functional groups on the bead surface and pollutants enhances adsorption efficacy.[81] In another study, Wang *et al.* observed changes in the adsorption rate with varying solution pH. The study examined $MgFe_2O_4$–BM–La(b) for phosphate removal over a pH range of 2–12. At acidic conditions, adsorption capacity increased until reaching a pH of 2.8, where the adsorption reached 35.36 mg g^{-1}. With a further increase in pH, adsorption capacity decreases.[77] Similarly, Wei *et al.* show that $Sb(OH)_6^-$ adsorption is low under acidic condition owing to excessive release of protons. In contrast, adsorption rate starts increasing at high pH due to negatively charged $Sb(OH)_6^-$ anions and positively charged surface.[78] The study by Afzal *et al.* shows the maximum adsorption of ciprofloxacin (CIP) using chitosan/biochar hydrogel beads at pH 5. At high pH values, the adsorbent shows a decrease in adsorption capacity due to occupation of active sites. At pH values 3–7, the surface of the adsorbent is negatively charged, which enhance the electrostatic interaction between adsorbent and CIP.[94] Also, Li *et al.* investigated the sludge-based magnetic gel beads for the removal of phosphorus using the macro–micro hybrid method. The study observed that

phosphate ions exhibit different dissociation constants, which change with the solution pH. The pH dissociates at 2.13, 7.20, and 12.36 in which the study revealed that the positively charged surface of biochar attracts negatively charged anions of phosphate ($H_2PO_4^-$ and HPO_4^{2-}). At high pH values, the negative charge on the phosphate increases, and the adsorption also increases from pH 2–8. However, as pH exceeds 8.55, the increasing negative charge on phosphate ions leads to electrostatic repulsion between the biochar surface and phosphate ions resulting in decreased adsorption efficiency.[95] The study by Küçük *et al.* also reveals that increasing the pH enhances the adsorption rate of MB dye. Furthermore, increasing the adsorbent dosage from also improves the adsorption performance owing to availability of binding sites on the BCA-Mag/AB surface.[90] Another study within a pH range of 3–9 reported maximum adsorption of STZ at pH 5.0. The maximum adsorption is found at pH 5, after which it decreases with a further increase in the pH of the solution. At pH 5, the adsorption capacity of CBC–Fe was 78.21 mg g^{-1}, which was higher compared to BC and CBC alone. At pH > 5, the adsorption capacity continuously decreased compared to other adsorbents. CBC–Fe shows 83% of removal rate after 1140 minutes which was higher than efficiencies of CBC and Fe.[83]

3.2.2 Effect of contact time. According to the study of Fan *et al.*, the adsorption performance is strongly influenced with the variation occur in contact time. The mCSB/SA adsorbent exhibit continuous increase in adsorption capacity 50 to 160 minutes and reached equilibrium at 400 minutes with the adsorption capacity of 124.0 mg g^{-1}.[54] The study by Ben Salem *et al.* observed the effect of contact time from 5 to 360 minutes to observe the fast adsorption process of prepared magnetic beads. In the beginning, the adsorption process increases up to 92% of the adsorption rate till 60 minutes. The adsorption rate attained equilibrium at 180 minutes, after which no increase in adsorption efficiency was observed for Cu^{2+} ions.[82] In another study, the adsorption process was carried out using pH 8.5 at time intervals of 5–90 minutes. Initially, the adsorption efficiency was fast owing to the availability of a large number of active sites. During the starting stage, the adsorption capacity reached 373.320 mg g^{-1}, resulting in physical adsorption. After this equilibrium starts reaching, the highest adsorption reached 392.92 mg g^{-1}, following chemisorption.[89] The study by Küçük *et al.*, found that with increase in time from 20 minutes to 180 minutes, the removal efficiency also increased. The longer the time, the dye molecules have more chances to enter the pores of BCA-Mag/AB and stick inside.[90]

3.2.3 Temperature. Temperature is a critical factor influencing the adsorption performance of biochar-based beads, as it directly affects reaction kinetics and adsorption processes. In the study by Fan *et al.*, observed a decrease in adsorption efficacy with an increased temperature which was directed by thermodynamics.[54] In another study, Zou shows that with an increase in temperature, the removal efficiency rises from 89.27% to 93.35% for FCB beads/H_2O_2 and from 88.09% to 93.23% for FCH beads/H_2O_2. This increase occurs because higher temperatures provide more energy, which activates H_2O_2 to generate $^{\bullet}OH$ radicals. As a result, collisions between the pollutant and free radicals increase, enhancing the removal efficiency.[79] Furthermore, the adsorption efficacy of the Ca-alginate–bentonite/biochar composite was investigated by Das *et al.* observing the change within 25 to 40 °C of temperature range. This improvement in the adsorption efficacy is associated with the enhanced solubility of particles, driven by increased Brownian motion.[80] Also, Qiao *et al.*, investigated the degradation of polycyclic aromatic hydrocarbons using a microbial consortium in biochar gel beads. The study optimized the temperature of gel beads from 15–35 °C to observe the high degradation efficiency. The degradation efficiency of HMW-PAHs increases with increasing temperature and reaches a maxima at 30 °C.[98] Furthermore, He *et al.* reported an increase in temperature also increase the adsorption potential by varying temperature ranges. Among all, the maximum adsorption reached 769.2 mg g^{-1} at 25 °C. Even at low temperatures, the prepared composite demonstrated high adsorption performance, which highlights its applicability over a broad temperature range and its potential for wastewater treatment.[92]

3.2.4 Adsorbent dosage. Adsorbent dosage is also one of the important parameter in adsorption studies, as it directly governs the availability of active sites. Consequently, various studies have investigated the influence of adsorbent dosage on the adsorption process. For instance, as per the study by Zou *et al.*, increasing the adsorbent dosage leads to improvement in removal efficiency. In this study, the removal efficiency of 40.78% was observed at 0.1 g L^{-1} of concentration of adsorbent, and 77.44% at 0.5 g L^{-1} removal rate for oxytetracycline hydrochloride. This increase in removal rate was attributed to the increase in available active sites with higher adsorbent dosage. The removal rate was maintained up to 92.43% by increasing the concentration of adsorbent from 0.1–0.5 g L^{-1}. However, after a further increase in adsorbent dosage, the adsorption efficacy decreases due to the blockage of active sites, leading to a decrease in the adsorption rate. This decrease in adsorption rate was attributed to the overlap or aggregation of active sites.[79] Similarly, in a study by Das *et al.*, the adsorption capacity increased with higher dosage, rising from 0.5 g to 1.5 g L^{-1}, due to the presence of more active pores. Nonetheless, after a certain point, further increases in the adsorbent dosage led to a decrease in adsorption efficacy, with the capacity dropping from 43.2 to 16.55 mg g^{-1}.[80] Also, Wang *et al.* observed the effect of adsorbent dosage on the removal of Cd(II) ions by varying the CA-BMB dosage. Initially, the increase in adsorbent dosage enhances the adsorption of Cd(II) ions due to the larger availability of active sites. The removal of Cd(II) ions increases sharply up to a certain limit attributed to the enlarged surface area. After reaching the maximum value, the removal efficiency declines as active sites become saturated. Another possible reason is the aggregation of particles at high concentrations, which reduces the total surface area.[88] Moreover, He *et al.* found that increasing the adsorbent dosage also increase removal rate of phosphate. When the adsorbent dosage was increased from 30 mg g^{-1} to 41 mg g^{-1}, the removal efficiency also increased from 36% to 94%. This occurs as the adsorbent amount offers greater adsorption sites. The study also suggests that when the adsorbent dosage was further increased, the adsorption

capacity declines attributed to the aggregation of polymeric materials. The study selected 50 mg of adsorbent for better adsorption.[91] Additionally, the adsorbent dosage highly affects the adsorption potential of LFX demonstrated by Mosaffa *et al.* in which the high dosage of LFX led to an increase in the interaction of LFX molecules with active sites. On the other hand, low adsorbent dosage limits their interaction, which results in the attainment of equilibrium. The results from this study reveal that attainment of equilibrium slows down with a rise in dosage, which leads to better possible interactions with adsorbate species.[89]

3.2.5 Initial concentration of pollutant. Numerous studies have reported that varying the initial concentration significantly influences the adsorption capacity of the prepared adsorbent. In particular, to find out the mechanism involved during the adsorption process and the type of interaction involved in the study, the impact of initial concentration provides insights. The study revealed that the adsorption potential of the prepared adsorbent increases with an increase in the initial concentration of Cr(VI) and reached a maximum at 769.2 mg g^{-1}.[92] The concentration was varied up to 500 mg L^{-1}, which revealed that (ii) at low concentration from 2–200 mg L^{-1}, both the removal efficiency and adsorption capacity increase. The obtained removal efficiency was 87.82% at the 200 mg L^{-1} concentration. This happens due to the presence of a large number of vacant active sites and less competition between the adsorbing molecules for adsorption. The prepared beads at the pH of 8.5 have a large surface area with positive sites that attract the negatively charged LFX. (ii) At high concentration (200 to 500 mg L^{-1}), the removal efficiency starts decreasing due to the limited vacant sites left on the surface of the adsorbent. After the adsorption of LFX molecules, the adsorbent surface gets saturated, leading to no more space left for adsorption.[89] Furthermore, the study by Jacob *et al.*, optimized the initial concentration of chlorpyrifos by varying it from 10, 30, and 50 ppm to obtain maximum adsorption capacity. The study suggests that an increase in concentration facilitates the faster breakthrough, with extended adsorption times observed to be 540, 600, and 570 minutes, respectively.[84]

4. Regeneration and recyclability of biochar-based beads

Desorption and regeneration of the adsorbent play a significant role in ensuring sustainability, cost-effectiveness, and large-scale applications. The regeneration of adsorbent is the process of removing adsorbed pollutants from the adsorbent material, which makes it reusable for further cycles of pollutant removal. Several studies have determined the regeneration process of the prepared adsorbent to ensure its large-scale applications. For instance, Afzal *et al.*, investigated the use of chitosan/biochar hydrogel beads for the removal of ciprofloxacin. In their study, 0.1 N NaOH was utilized as an eluent for the recyclability and reusability of the prepared adsorbent. Their results demonstrate the removal of ciprofloxacin up to six adsorption–desorption cycles with a slight reduction in adsorption capacity. The study indicated that the reduction in adsorption capacity was mainly due to the loss of functional groups on the surface of the adsorbent during the regeneration process.[94] Similarly, in another instance, Fan *et al.* reveal a slight decrease in the adsorption rate in five adsorption cycles. Specifically, the adsorption performance decreases using HCl eluent from 99.2% to 95.4% after five to desorb the methylene blue from the surface of the adsorbent.[54] The study by Zou *et al.* reported iron-doped biochar beads and hydrogel beads for the removal of oxytetracycline hydrochloride (OTC) using coffee grounds as natural precursors. In this study, the authors utilized H_2O_2 as a catalyst to enhance the beads' ability to remove OTC from aqueous solutions. The results showed that study observed a 91% removal efficacy within 60 minutes. The reduction in removal efficiency occurs due to the slight leaching of iron ions from the surface of the catalyst, leading to a reduction in active sites.[79] Furthermore, another study of the reusability of prepared magnetic biochar-based beads was conducted by Ben Salem *et al.*, using 0.1 M NaOH as a desorbing agent. In this study, adsorption was maintained up to 3 cycles with a slight decrease in adsorption efficacy from 66.6% to 55.3% with varying concentrations of Cu^{2+} ions.[82] Specifically, the adsorption efficacy of Cu^{2+} metal ions was observed at 60.1% at copper metal ion concentrations of 200 mg L^{-1}, 88.70%, and 78.46% at 50 mg L^{-1} for the desorption conducted by NaOH and HCl, respectively. Moreover, in another study, 0.1 M HCl was utilized as a desorbing agent, in which the adsorbent remains stable up to 4 adsorption–desorption cycles. The adsorption experiment was carried out by mixing 0.2 g of the BC/Alg composite beads in a 20 mL of MB dye solution. After the addition of beads, the mixture was continuously stirred for 50 minutes to make the methylene blue completely attached to the adsorbent surface.[93] Furthermore, the recyclability of SA-KBC-Fe/La was assessed after 5 consecutive adsorption–desorption cycles. The sorption capacity was found to be 43.19 mg g^{-1} for the first cycle, which gradually decreased to 35.48 mg g^{-1} by the fifth cycle.[91] Finally, the regeneration potential of the prepared adsorbent in another study by Jacob *et al.* was tested by using it multiple times, which exhibits stability up to 6 adsorption–desorption cycles. In the first cycle, the desorption rate was found to be 90% which was reduced to 60% in the sixth cycle. This decrease in removal efficiency was attributed to the blockage of pores, which reduces sorption sites.[99] Overall, these findings highlight that the prepared adsorbents exhibit promising regeneration performance with minimal loss in adsorption capacity over multiple cycles. Table 2 illustrates the regeneration performance of various biochar-based bead adsorbents.

5. Comparison of biochar-based bead performance with powdered biochar composites and other adsorbents

In past decades, water pollution has become a major concern due to increasing population growth, economic development,

Table 2 Comparison of the regeneration performance of various biochar-based bead adsorbents

S/N	Adsorbent	Eluent	Number of cycles	Adsorption capacity	Adsorption capacity (after regeneration)	Ref.
1	Chitosan/biochar hydrogel beads	1.0 N NaOH	6	36.72 mg g^{-1}	25.73 mg g^{-1}	94
2	Biochar/polyaniline/alginate composite beads	—	5	821 mg g^{-1}	821 mg g^{-1}	87
3	Magnetic-biochar/alginate bead	0.1 M NaOH	3	—	—	82
4	Fe_3O_4-modified coconut shells/sodium alginate aerogel beads	0.5 M HCl	5	—	—	54
5	Modified biochar beads	NaOH	5	255.88 mg g^{-1}	—	86
6	CS/PVA–BC@CoNiAl-LDH beads	NaOH	6	—	—	89
7	BC/Alg composite	0.1 M HCl	4	—	—	93
8	Biochar/alginate beads	0.1 M NaOH	6	318 mg g^{-1}	148 mg g^{-1}	92
9	Sugarcane bagasse-based biochar alginate beads	NaOH	6	—	—	84
10	SA-KBC-Fe/La beads	—	5	43.19 mg g^{-1}	35.48 mg g^{-1}	91

and largely increasing industrial activities to fulfill human needs. Water pollution has become a serious global threat, and there is an urgent need to take steps to minimize it and to use advanced methods to clean wastewater. Several studies have reported that wastewater treatment using biochar-based composites in their powdered form exhibits higher adsorption capacities due to their smaller size and large surface area. However, despite these advantages, powdered form of biochar presents difficulty in real-time applications in terms of separation and recovery from treated solutions. To separate the biochar from treated solutions requires additional processes, including centrifugation, which is difficult on a large scale. To overcome these challenges, recent work has focused on the preparation of biochar-based beads, which have a lower surface area compared to the powdered form of biochar and are easy to handle. The beads are present in a solid and discrete form, making them more suitable for industrial applications. Several studies have reported that bead structure exhibits higher stability and improved reusability compared to the powdered form of biochar-based composites. For instance, Wei *et al.* reported Sb(v) removal using magnetic $MgFe_2O_4$-biochar composite beads. Their results demonstrates that Fe/(MgFeO–BC) beads provided high stability and get easily separated compared to their powdered form. The adsorption capacity of bare biochar is less than 23.38 mg g^{-1} due to less active sites compared to beads having large active sites.[78] In contrast to other reported natural adsorbents, biochar-based adsorbents exhibit high adsorption capacity due to their unique properties having a highly porous structure and larger surface area. Other natural adsorbents, including clay, zeolite exhibit low adsorption capacities over biochar-based composites. Moreover, biochar-based composites are cost-effective prepared using natural precursors mostly from agricultural residues, compared to other adsorbents including activated carbon, zeolites which is more expensive due to its production process. To further enhance the adsorption capacities, biochar-based composites can be functionalized by introducing surface groups such as carboxyl, hydroxyl, and carbonyl moieties onto the adsorbent. The most important thing is biochar-based adsorbents are reusable and can be easily regenerated to re-treat the wastewater. In contrast, recovering the activated carbon, and powdered biochar is challenging which restricts their real time applications. Magnetic biochar-based beads, however, are not only reusable and cost-effective but also suitable for large-scale and industrial applications. For instance, Wang *et al.* investigated calcium-alginate biochar beads to improve the removal rate of Cd(II) ions. The study found a maximum adsorption capacity of 227.1 mg g^{-1} for the prepared adsorbent. To evaluate the influence of different adsorbents, the study compared calcium-alginate (CA), calcium-alginate incorporated with ball-milled biochar (CA-BMB), and bare ball-milled biochar. The results showed that the adsorption capacities were 251.8 mg g^{-1} for CA-BMB, 227.1 mg g^{-1} for CA, and 40.0 mg g^{-1} for ball-milled biochar, respectively. The bare ball-milled biochar exhibited an adsorption capacity of only 40.0 mg g^{-1} for Cd(II) ions, which is significantly lower than the 227.1 mg g^{-1} observed for the calcium-alginate ball-milled biochar beads.[88] Similarly, Fan *et al.*, prepared CSB/SA for the effective adsorption of methylene blue for wastewater treatment. The modified aerogel beads facilitate high adsorption rate and easy separation compared to powdered form adsorbents.[54] In another study, the modification of sodium alginate beads also enhances the adsorption capacity compared to bare beads. The authors reported that EC-Alg/PEI-3 exhibited 51.8 m^2 g^{-1} of surface area, significantly higher than the unmodified beads. Simultaneously, the pore volume of the adsorbent increases with an increase in pore size from 12.1 nm to 26.4 nm. With occupancy of active sites, the pore size, volume, and surface area starts reducing. Moreover, the modified material EC-Alg/PEI-3 contained more active sites compared to unmodified biochar. For example, the surface area of bare biochar was 79.711 m^2 g^{-1}, which was much less compared to Mg-modified biochar having 308.120 m^2 g^{-1}.[92] Furthermore, Faouzia *et al.* prepared biochar/polyaniline/alginate composite beads (ABC–PA–SG) using *Crataegus azarolus* seed (CAS) waste as a natural precursor for removal of MB. Their study utilized a calcination process, which enhanced the ash content of the natural precursor (CAS) in the activated biochar samples. Initially, the ash content was 0.64%,

which increased to 2.3% due to the release of carbon during thermal decomposition.[87] The prepared samples featured mesopores of 2–50 nm and mesopores with a size >50 nm. The modification of biochar yielded enhanced adsorption capacity. For instance, pristine biochar was found to have a less porous structure and negligible surface area. After functionalization, the pore diameter increased up to ~2–3 nm. Although bare biomass contains several functional groups, its low surface area results in pore adsorption capacity. To determine the maximum adsorption capacity, the study optimized parameters such as pH, concentration of methylene blue, and temperature conditions. The results revealed an enhancement in sorption capacity at a methylene blue concentration of 100 mg L^{-1} and a pH of 6.4 at room temperature. These findings demonstrate that biochar-based bead adsorbents offer promising results over the powdered form of biochar, combining ease of separation, high stability for real-world water purification processes.

6. Conclusion and future perspectives

Biochar-based beads are gaining attention as efficient materials for wastewater treatment owing to their distinctive surface properties and eco-friendly nature. The incorporation of magnetic materials, polymer matrices, and clay materials enhances the density of functional groups on the adsorbent surface and can improve the structural stability and adsorption performance of bead-based adsorbents. Although bead formation may decrease the surface area compared to powdered biochar, it significantly enhances recovery, handling, and reusability, making beads more suitable for practical and large-scale applications.

This review highlights recent advances in synthesis approaches, natural precursors, and structural integrity of biochar-based beads. Furthermore, the study discusses the adsorption mechanisms including electrostatic interaction, hydrogen bonding, π–π stacking, ligand exchange, and redox processes, and assesses their effectiveness in the removal of a wide range of pollutants such as heavy metals, dyes, and organic contaminants. Some studies follow synergistic interactions that significantly enhance the adsorption performance and broaden their applications for different types of contaminants. Despite this, to further strengthen the applicability of biochar-based beads, several key aspects remain unexplored. Subsequent studies may emphasize the selectivity of fabricated adsorbents towards specific types of contaminants by tailoring their functional groups. Moreover, it is essential to improve the regeneration ability of adsorbents, which is crucial to make the material cost-effective. The optimization of these materials under different environmental conditions remains unexplored. Various studies have yet to work on the lab-scale, so scaling up the production to the industrial level by introducing continuous flow or fixed-bed systems into beads will be vital for practical deployment. In addition to this future work should be focus on addressing the potential mass-transfer limitation with intra-particle diffusion within the beads. The hydraulic performance and pressure drop behavior of bead-based adsorbents must also be evaluated. In order to avoid secondary contamination, mechanical integrity during extended operational stress and multiple regeneration cycles, as well as the possibility of long-term leaching of polymeric binders or integrated metal components, should be carefully examined.

Moreover, understanding the long-term impact, toxicity, and complex formation of these adsorbents on the environment is crucial. Interdisciplinary approaches combining computational modelling, environmental engineering, and material science can drive the development of next-generation biochar-based beads for efficient, affordable, and sustainable water treatment technologies.

Conflicts of interest

There are no conflicts to declare.

Abbreviations

FCB	Ferric crosslinked alginate-based biochar beads
FCH	Ferric crosslinked alginate-based hydrogel beads
CA–B/ABC beads	Calcium alginate–bentonite/activated biochar composite
BAB	Biochar alginate beads
EDA interactions	Electron donor–acceptor interactions
SA/H_3PO_4-activated CC-ABC	Sodium alginate/H_3PO_4 activated corncob-based biochar composite beads
LDH–BC/CS–PVA beads	LDH–biochar cross-linked chitosan/PVA beads
AFB/Alg beads	Amino-functionalized biochar/alginate beads
CSB/SA	Coconut shell biochar/sodium alginate composite aerogel beads

Data availability

No primary research results, software or code have been included and no new data were generated or analysed as part of this review.

Acknowledgements

The authors gratefully acknowledge Rayat Bahra University, India, for providing the necessary resources for the study.

References

1 B. Sarker, K. N. Keya, F. I. Mahir, K. M. Nahiun, S. Shahida and R. A. Khan, *Sci. Rev.*, 2021, **7**, 32.
2 M. Moore, P. Gould and B. S. Keary, *Int. J. Hyg. Environ. Health*, 2003, **206**, 269.
3 A. J. McMichael, *Bull. W. H. O.*, 2000, **78**, 1117.

4 K. Jayaswal, V. Sahu, and B. R. Gurjar, in *Water Remediat.*, Springer, 2017, pp. 11–27.
5 R. P. Schwarzenbach, T. Egli, T. B. Hofstetter, U. Von Gunten and B. Wehrli, *Annu. Rev. Environ. Resour.*, 2010, **35**, 109.
6 M. A. ul Hassan Rashid, M. M. Manzoor and S. Mukhtar, *Asian J. Water, Environ. Pollut.*, 2018, **15**, 67.
7 J. Singh, P. Yadav, A. K. Pal, and V. Mishra, in *Sensors Water Pollut. Monit. Role Mater.*, Springer, 2019, pp. 5–20.
8 S. Madhav, A. Ahamad, A. K. Singh, J. Kushawaha, J. S. Chauhan, S. Sharma, and P. Singh, *Sensors Water Pollut. Monit. Role Mater.*, 2019, vol. 43.
9 K. Hikmat, H. Aziz, F. S. Mustafa and K. M. Omer, *RSC Adv.*, 2023, 17595.
10 K. H. H. Aziz, *Desalin. Water Treat.*, 2024, 100757.
11 M. R. Singh and A. Gupta, *Water pollution-sources, effects and control*, Cent. Biodiversity, Dep. Bot. Nagal. Univ., 2016, vol. 1.
12 I. Zahoor and A. Mushtaq, *Int. J. Chem. Biochem. Sci*, 2023, **23**, 164.
13 N. E. Peters and M. Meybeck, *Water Int.*, 2000, **25**, 185.
14 M. Padhiary and R. Kumar, in *Smart Internet Things Environ. Healthc.*, Springer, 2024, pp. 107–126.
15 K. Hikmat, H. Aziz and N. M. Fatah, *R. Soc. Open Sci.*, 2026, 232033.
16 WHO, *Drinking-water*, 2023, https://www.who.int/news-room/fact-sheets/detail/drinking-water.
17 D. Vanham, L. Alfieri, M. Flörke, S. Grimaldi, V. Lorini, A. de Roo and L. Feyen, *Lancet Planet. Heath*, 2021, **5**, e766.
18 B. S. Lal, *Int. J. Sci. Res.*, 2019, **8**, 1949.
19 K. Annan and U. N. Secretary-General, RECOGNIZING Prev. Dis. Inj.
20 K. Szálkai, in *Palgrave Encycl. Glob. Secur. Stud.*, Springer, 2023, pp. 319–326.
21 M. E. Assessment, *Ecosystems and Human Well-Being: Wetlands and Water*, World resources institute, 2005.
22 C. Corvalan, S. Hales, and A. J. McMichael, *Ecosystems and Human Well-Being: Health Synthesis*, World Health Organization, 2005.
23 WHO, *Drinking-water*, 2023, https://www.who.int/news-room/fact-sheets/detail/drinking-water.
24 A. Shrivastav and P. Singh, *Curr. Probl. Cardiol.*, 2024, **49**, 102120.
25 R. Chowdhury, A. Ramond, L. M. O'Keeffe, S. Shahzad, S. K. Kunutsor, T. Muka, J. Gregson, P. Willeit, S. Warnakula and H. Khan, *BMJ*, 2018, **362**, k3310.
26 A. Sonune and R. Ghate, *Desalination*, 2004, **167**, 55.
27 H. Sukmana, N. Bellahsen, F. Pantoja and C. Hodur, *Prog. Agric. Eng. Sci.*, 2021, **17**, 49.
28 E. Obotey Ezugbe and S. Rathilal, *Membranes*, 2020, **10**, 89.
29 K. Hikmat, H. Aziz, F. S. Mustafa, R. Fayaq and K. M. Omer, *J. Water Process Eng.*, 2025, **70**, 106867.
30 M. N. Rashed, in *Org. Pollut. Risk Treat.*, IntechOpen, 2013.
31 S. Rajendran, A. K. Priya, P. S. Kumar, T. K. A. Hoang, K. Sekar, K. Y. Chong, K. S. Khoo, H. S. Ng and P. L. Show, *Chemosphere*, 2022, **303**, 135146.
32 K. Hikmat, H. Aziz, F. S. Mustafa and S. Hama, *Coord. Chem. Rev.*, 2025, **542**, 216875.
33 H. Soni, M. Bhattu, S. D. Priya, M. Kaur, M. Verma and J. Singh, *Environ. Res.*, 2024, **251**, 118560.
34 H. Kaur, M. Bhattu, S. Chakroborty, M. K. Aulakh, V. Mutreja, M. Verma, K. Tiwari, C. Chakraborty and I. A. Darwish, *ACS Omega*, 2025, **10**, 2354.
35 H. Soni, V. Jain, S. Ballal, I. A. Ariffin, M. Chahar, S. Saini, M. Bhattu, H. Singh, M. Bechelany and J. Singh, *Nanomaterials*, 2024, **14**, 1766.
36 D. Kathuria, M. Bhattu, A. Bankar and P. Puri, *ChemistrySelect*, 2023, **8**, e202302293.
37 J. Singh, M. Bhattu and M. Verma, *Top. Catal.*, 2025, **68**, 573.
38 J. Singh, M. Bhattu, M. Verma, M. Bechelany, S. K. Brar and R. Jadeja, *Nanomaterials*, 2025, **15**, 66.
39 M. B. Shakoor, S. Ali, M. Rizwan, F. Abbas, I. Bibi, M. Riaz, U. Khalil, N. K. Niazi and J. Rinklebe, *Int. J. Phytorem.*, 2020, **22**, 111.
40 S. Dwivedi and S. Dey, *Int. J. Environ. Sci. Technol.*, 2023, **20**, 9335.
41 K. Hikmat, H. Aziz, F. S. Mustafa, M. A. H. Karim and S. Hama, *J. Environ. Manage.*, 2025, **390**, 126245.
42 K. H. H. Aziz, in *Advanced Technologies for the Removal of Heavy Metals from Industrial Effluents*, CRC Press, 2025, pp. 15–31.
43 C. V Putnis and A. Putnis, *J. Cryst. Growth*, 2022, **600**, 126840.
44 K. P. Ananthapadmanabhan and P. Somasundaran, *Colloids Surf.*, 1985, **13**, 151.
45 H. Peng and J. Guo, *Environ. Chem. Lett.*, 2020, **18**, 2055.
46 S. A. Abdalla, F. S. Mustafa, K. Hikmat, H. Aziz, S. J. Mohammed and D. A. Kader, *RSC Adv.*, 2025, 42843.
47 R. Kareem, A. Afkhami and K. H. H. Aziz, *ChemistrySelect*, 2025, **10**, e03708.
48 C. Ii, 2025, p. 20309.
49 V. Phouthavong, R. Yan, S. Nijpanich, T. Hagio, R. Ichino, L. Kong and L. Li, *Materials*, 2022, **15**, 1053.
50 R. N. Noori, D. F. Hamamin and K. H. H. Aziz, *J. Dispersion Sci. Technol.*, 2025, **1**, 1–13.
51 R. K. Sharma, T. P. Singh, S. Mandal, D. Azad, and S. Kumar, in *Eng. Biochar Fundam. Prep. Charact. Appl.*, Springer, 2022, pp. 65–84.
52 P. Anerao, G. Salwatkar, M. Kumar, A. Pandey, and L. Singh, in *Eng. Biochar Fundam. Prep. Charact. Appl.*, Springer, 2022, pp. 49–64.
53 K. Hikmat and H. Aziz, *4 – Biochar, Hydrochar, and Their Derivative Composites for Heavy Metal Adsorption*, Elsevier, 2026.
54 W. Fan and X. Zhang, *Int. J. Biol. Macromol.*, 2025, **284**, 137945.
55 O. S. Olugbenga, P. G. Adeleye, S. B. Oladipupo, A. T. Adeleye and K. I. John, *Waste Manag. Bull.*, 2024, **1**, 1.
56 B. Díaz, A. Sommer-Márquez, P. E. Ordoñez, E. Bastardo-González, M. Ricaurte and C. Navas-Cárdenas, *Resources*, 2024, **13**, 8.
57 W. Kwapinski, C. M. P. Byrne, E. Kryachko, P. Wolfram, C. Adley, J. J. Leahy, E. H. Novotny and M. H. B. Hayes, *Waste Biomass Valorization*, 2010, **1**, 177.
58 S. Wijitkosum, *Int. Soil Water Conserv. Res.*, 2022, **10**, 335.

59 X. Yang, H. Wang, P. J. Strong, S. Xu, S. Liu, K. Lu, K. Sheng, J. Guo, L. Che and L. He, *Energies*, 2017, **10**, 469.
60 M. Tripathi, M. N. Mujawar and P. Ganesan, *Overview on Synthesis of Magnetic Bio Char from Discarded Agricultural Biomass*, 2016, ch. 16.
61 A. A. Burbano, G. Gascó, F. Horst, V. Lassalle and A. Méndez, *Biomass Bioenergy*, 2023, **172**, 106772.
62 L. R. Marcelo, J. S. de Gois, A. A. da Silva and D. V. Cesar, *Environ. Chem. Lett.*, 2021, **19**, 1229.
63 L. Tang, J. Yu, Y. Pang, G. Zeng, Y. Deng, J. Wang, X. Ren, S. Ye, B. Peng and H. Feng, *Chem. Eng. J.*, 2018, **336**, 160.
64 P. Singh, A. K. Singh, V. K. Singh, and V. Kumar, *Nanotechnology-Based Sustainable Agriculture*, Wiley Online Library, 2025.
65 S. Jahan, U. e Habiba, M. Akbar, M. Zafar, A. A. Shah and S. O. Alomrani, *J. Soil Sci. Plant Nutr.*, 2024, **24**, 4755.
66 Y. Li, X. Zhang, H. H. Ngo, W. Guo, T. Long, H. T. Wen and D. Zhang, *J. Membr. Sci.*, 2023, **670**, 121383.
67 T. Arima, K. Idemitsu, K. Yamahira, S. Torikai and Y. Inagaki, *J. Alloys Compd.*, 2005, **394**, 271.
68 R. Petrović, N. Tanasković, V. Djokić, Ž. Radovanović, I. Janković-Častvan, I. Stamenković and D. Janaćković, *Powder Technol.*, 2012, **219**, 239.
69 Q. Guo, E. R. Bandala, A. Goonetilleke, N. Hong, Y. Li and A. Liu, *J. Water Process Eng.*, 2021, **40**, 101892.
70 L. E. Nielsen, *J. Macromol. Sci., Part C*, 1969, **3**, 69.
71 X. Li, W. Zhang, Y.-C. Wang, W. Zhang, H.-Q. Wang and J. Fang, *Nat. Commun.*, 2018, **9**, 3806.
72 C. Tang, C. D. Saquing, J. R. Harding and S. A. Khan, *Macromolecules*, 2010, **43**, 630.
73 T. Hanein, K.-C. Thienel, F. Zunino, A. T. M. Marsh, M. Maier, B. Wang, M. Canut, M. C. G. Juenger, M. Ben Haha and F. Avet, *Mater. Struct.*, 2022, **55**, 3.
74 B. Rand, in *Concise Encycl. Adv. Ceram. Mater.* , Elsevier, 1991, pp. 49–51.
75 Y. Lu, H. Wang, Y.-Y. Lu, Z.-Q. Ren, N. Gao, J.-J. Wang, B.-C. Huang and R.-C. Jin, *J. Environ. Manage.*, 2025, **373**, 123607.
76 B. Li, X. Zhou, N. Su and Q. Zhao, *Surf. Interfaces*, 2025, 107174.
77 L. Wang, J. Wang, W. Yan, C. He and Y. Shi, *Chem. Eng. J.*, 2020, **387**, 123305.
78 H. Li, Y. Wei, Y. Wang, Y. Zhao, L. Wang, J. Feng and F. Sun, *Colloids Surf., A*, 2024, **684**, 133133.
79 W. Zou, M. Zhang, X. Zhang, D. Zhang, C. Li, L. Zhong, W. Guo and H. H. Ngo, *J. Water Process Eng.*, 2025, **69**, 106723.
80 L. Das, N. Saha, A. Ganguli, P. Das, A. Bhowal and C. Bhattacharjee, *Environ. Technol. Innovation*, 2021, **24**, 101955.
81 B. Hu, N. Yan, Z. Zheng, L. Xu, H. Xie and J. Chen, *Nanomaterials*, 2023, **13**, 1.
82 D. Ben Salem, A. Ouakouak, F. Touahra, N. Hamdi, A. S. Eltaweil, A. Syed, R. Boopathy and H. N. Tran, *Bioresour. Technol.*, 2023, **383**, 129225.
83 M. I. Al-Wabel, M. Ahmad, A. R. A. Usman and A. S. F. Al-Farraj, *Saudi J. Biol. Sci.*, 2021, **28**, 6218.
84 M. M. Jacob, M. Ponnuchamy, A. Kapoor and P. Sivaraman, *Environ. Res.*, 2025, **269**, 120902.
85 S. Kang, S. M. Park, J. G. Park and K. Baek, *J. Environ. Manage.*, 2019, **234**, 181.
86 X. Fu, P. Wang, P. Zheng, T. Wang, X. Li and M. Ren, *J. Environ. Chem. Eng.*, 2022, 108177.
87 B. Faouzia, K. Imene, H. Chaima, B. Riadh, B. A. Imene, A. Gil, B. Mokhtar and B. C. Eddine, *Int. J. Biol. Macromol.*, 2025, **305**, 141338.
88 B. Wang, B. Gao and Y. Wan, *J. Ind. Eng. Chem.*, 2018, **61**, 161.
89 E. Mosaffa, E. Jamshidi, H. Patel, F. Manteghi, H. Ghafuri, B. A. Kikani and A. Banerjee, *Desalination*, 2025, **599**, 118452.
90 İ. Küçük and N. Yıldız Küçük, *Appl. Sci.*, 2025, **15**, 2085.
91 D. He, Z. Zhang, W. Zhang, H. Zhang and J. Liu, *Int. J. Biol. Macromol.*, 2024, **261**, 129732.
92 Y. He, J. Chen, J. Lv, Y. Huang, S. Zhou, W. Li, Y. Li, F. Chang, H. Zhang, T. Wågberg and G. Hu, *J. Cleaner Prod.*, 2022, **373**, 133790.
93 K. Bahsaine, H. Benzeid, N. Zari, A. e. K. Qaiss and R. Bouhfid, *Int. J. Biol. Macromol.*, 2024, **282**, 136853.
94 M. Z. Afzal, X. F. Sun, J. Liu, C. Song, S. G. Wang and A. Javed, *Sci. Total Environ.*, 2018, **639**, 560.
95 H. Li, Y. Zhao, Z. Xiao, M. Yang and B. Zhou, *Chem. Eng. J.*, 2021, **422**, 130028.
96 J. Chen, J. Ouyang, X. Cai, X. Xing, L. Zhou, Z. Liu and D. Cai, *Sep. Purif. Technol.*, 2021, **276**.
97 G. Murtaza, Z. Ahmed, D.-Q. Dai, R. Iqbal, S. Bawazeer, M. Usman, M. Rizwan, J. Iqbal, M. I. Akram and A. S. Althubiani, *Front. Environ. Sci.*, 2022, **10**, 1035865.
98 K. Qiao, W. Tian, J. Bai, L. Wang, J. Zhao, T. Song and M. Chu, *Mar. Pollut. Bull.*, 2020, **159**, 111489.
99 M. Ponnuchamy, A. Kapoor, P. Senthil Kumar, D. V. N. Vo, A. Balakrishnan, M. Mariam Jacob, and P. Sivaraman, *Sustainable Adsorbents for the Removal of Pesticides from Water: A Review*, Springer International Publishing, 2021.